

# Novel Approach to Constructing an Ultra Low Cost Flowcell Biosensor

## THESIS

Presented to the Faculty of the Department of Physics and Astronomy  
in Partial Fulfillment of the Major Requirements  
for the Degree of

BACHELOR OF SCIENCE IN  
PHYSICS

Jeffery Summers

May 2019

©2019 Middle Tennessee State University

All rights reserved.

The author hereby grants to MTSU permission to reproduce  
and to distribute publicly paper and electronic  
copies of this thesis document in whole or in part  
in any medium now known or hereafter created.

Novel Approach to Constructing an Ultra Low Cost Flowcell Biosensor

Jeffery Summers

Signature of Author:

---

Department of Physics & Astronomy

May 2019

Certified by:

---

Dr. William Robertson

Department of Physics & Astronomy

Thesis Supervisor

Accepted by:

---

Dr. Ronald Henderson

Professor of Physics & Astronomy

Chair, Physics & Astronomy

## ABSTRACT

In this thesis we present our approach to constructing an ultra low-cost flowcell biosensor. Our sensor is capable of detecting changes in index of refraction on the order of  $10^{-3}$ , showing that it is well suited for not only index testing but also for surface loading type processes where binding between molecules may occur. Our sensor utilizes 3D printed parts, a one dimensional photonic crystal coupled to a glass prism (rather than a traditional SPR metal-film-prism coupling system), and a CCD to operate. Highly sensitive Bloch Surface Waves (BSWs) can be excited in the outer layer of our multilayer by coupling an incident laser beam to the prism-multilayer structure and the position of the BSWs can be tracked by analyzing the reflected beam. By using this method we are able to bring the cost of manufacturing the sensor to about \$100, excluding the photonic crystals which can be fabricated commercially. The largest cost of our system is the CCD used to collect data.

## TABLE OF CONTENTS

|                                   |     |
|-----------------------------------|-----|
| Abstract . . . . .                | iii |
| I. Introduction . . . . .         | 1   |
| II. Experimental Design . . . . . | 4   |
| III. Methods . . . . .            | 7   |
| IV. Results . . . . .             | 9   |
| V. Conclusion . . . . .           | 11  |
| VI. References . . . . .          | 12  |

## LIST OF FIGURES

|    |   |    |
|----|---|----|
| 1  | Surface Plasmon Resonance setup . . . . .   | 1  |
| 2  | The laser on the right side of the image couples into the prism-multilayer structure atop the centerpiece and is then reflected into a CCD where data can be taken. . . . .   | 2  |
| 3  | An illustration of the photonic crystal used in our sensor . . . . .  | 4  |
| 4  | Top: the beam holding the laser and focusing lens. Bottom: the beam holding the camera and neutral density filter. . . . .  | 4  |
| 5  | Primary stage and flowcell stage of our sensor. The green round 3D printed fixture underneath the flowcell is the primary stage which the two beams are attached to. The blue 3D printed piece mounted to the primary stage is the flowcell stage. The glass prism, multilayer, and flowcell chamber are attached atop the flowcell stage with the use of hex screws and 3D printed braces. . . . . | 5  |
| 6  | The flowcell stage, prism, multilayer and flowcell chamber. A rubber gasket is set in a groove around the chamber so that when the braces are tightened the interface between the multilar and flowcell is liquid tight. . . . .  | 6  |
| 7  | The theoretical relation between the angular position of the mode and the index of refraction inside the flowcell chamber. . . . .  | 8  |
| 8  | Index shift measurements for ethanol. . . . .   | 9  |
| 9  | Index shift measurements for acetone. . . . .   | 10 |
| 10 | Index shift measurements for 70% isopropyl alcohol. . . . .   | 10 |

## I. INTRODUCTION

Flowcell sensors have many applications; disease detection, refractive index measurements and measurements of reactivity to name a few. These sensors have been operating on the basis of electromagnetic surface phenomena for decades [1]. Most flowcells on the market work by exploiting surface plasma oscillations (SPOs). These oscillations are highly sensitive to changes in the optical properties of the adjacent medium and follow from Maxwell's equations when the dielectric functions of each medium satisfy the relation [2]

$$\frac{\epsilon_{spo}}{\epsilon_{adjacent}} < -1$$

Metals like aluminum, copper, gold, and silver have negative dielectric functions at wavelengths in the red/infrared [2], so films of these metals are used as to generate SPOs in most flowcell sensors via a process known as Surface Plasmon Resonance (SPR). An SPR system utilizes light-prism coupling to excite the surface electrons on a thin metal film deposited on the hypotenusal face of the prism. A dark band representing the photons absorbed by the

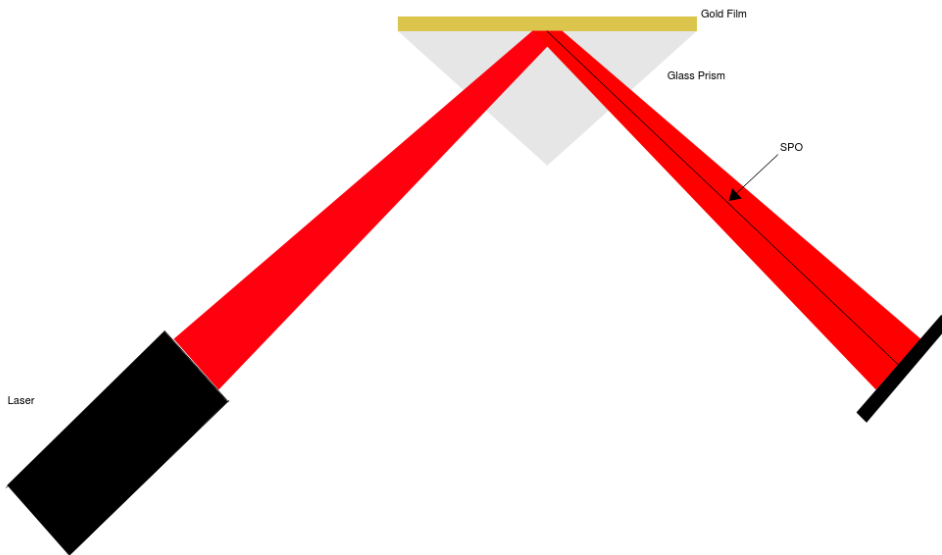


Figure 1: Surface Plasmon Resonance setup

surface electrons appears on the reflected beam image as seen in figure 1. There are quite a few drawbacks for using metal films, however. Metals are highly reactive so each time an SPR system is used a new prism must be used. These films also require particular wavelengths of incident light to excite the oscillations. Rather than using metal films, one-dimensional photonic crystals, or multilayers, can be designed to exhibit the phenomenon of surface electromagnetic waves (SEWs) or Bloch surface waves (BSWs), named after the physicist Felix Bloch who was famous for working with periodic systems. These surface waves have the same practical application as SPOs.

Multilayers overcome both of the shortcomings of metal films listed here. They can be designed to work for any wavelength and are typically made of nonreactive glass. Modular 3-D printed parts synthesize nicely with the flexible nature of multilayers, resulting in a sensor that is capable of working with many materials. In addition to these benefits, we expect that our 3-D printed and multilayer-based flowcell sensor will be more sensitive and precise with its measurements and be far cheaper to both build and maintain compared to traditional SPR sensors.

To take measurements with our sensor we look at the reflected image of incident laser light which has been coupled into the prism-multilayer interface to produce a BSW in the terminating layer. Our multilayer is designed to trap incident light in the last layer at a special angle; this results in a dark band in our reflected image. A diagram of the sensor is shown below.

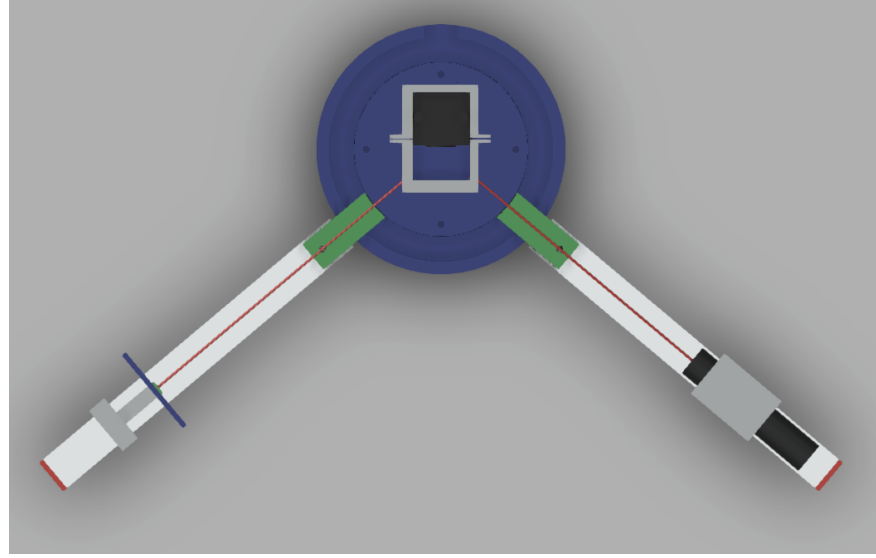


Figure 2: The laser on the right side of the image couples into the prism-multilayer structure atop the centerpiece and is then reflected into a CCD where data can be taken.

As fluids or gases are put into the flowcell chamber the index of refraction,  $n_c$ , changes. The condition for total internal reflection, found from Snell's law, for the interface between a glass prism and some transmitting medium whose index of refraction varies with time is given by:

$$\sin(\theta_c(t)) = \frac{n_c(t)}{n_g}$$

We obtain an expression for the angle of reflection as a function of time by the Law of Reflection:

$$\theta_r(t) = \arcsin \frac{n_c(t)}{n_g}$$

Note that this expression is only valid for a single interface and hence does not accurately reflect our setup as we use

a multilayer that behaves much differently than a single interface. With that said, this expression for  $\theta_r$  does capture the essence of our setup; the reflected angle (this is equivalent to the position of the surface mode) is a dependent on the index of refraction of the chamber. Using this fact we can associate variations in the flowcell chamber's refractive index with differences in the BSWs angular position. These angular differences can be calculated by tracking the variation in the position of the dark band in the reflected image. A detailed analysis relating a shift in pixels on the CCD to the angular variation of the surface mode is listed in the methods section.

To use this device for disease detection, or to detect any sort of biological binding process, the multilayer must have the binding agent in question deposited onto the outer layer. The characteristic of the surface mode is first captured with just the binding agent and an empty (or water filled) flowcell chamber. After acquiring the characteristic of the surface mode the molecules to be binded are then flushed through the chamber and if binding occurs the surface mode's characteristics will be different than before.

## II. Experimental Design

The process of design for this experiment relies heavily on the use of a 15 millimeter right prism and our photonic crystal. The photonic crystal is composed of 3 bilayers of TiO<sub>2</sub> and SiO<sub>2</sub>. The dielectric function of TiO<sub>2</sub> is taken as  $\epsilon_{TiO_2} = 4.84 + 0.0007i$  and the dielectric function of SiO<sub>2</sub> is taken as  $\epsilon_{SiO_2} = 2.1316 + 0.0001i$ .

It should be noted that the imaginary parts of each dielectric function may not be accurate and have been included to introduce some form of loss that fits the results of prior experiments. Figure 3 illustrates the structure of the multilayer. The basic design of the sensor is split into three different parts: the primary stage, two beams, and the flowcell stage. One of the two beams holds our laser and a focusing lens while the other holds the CCD and captures the reflected beam. Normally the laser light is too intense to pick up the surface mode in the reflected image. However, we attach a neutral density (d=3.5, see Figure 4) filter to reduce the intensity and this allows us to image the surface mode.

|              |
|--------------|
| 410.0nm SiO2 |
| 121.0nm TiO2 |
| 188.3nm SiO2 |
| 121.0nm TiO2 |
| 188.3nm SiO2 |
| 121.0nm TiO2 |
| 188.3nm SiO2 |

Figure 3: An illustration of the photonic crystal used in our sensor

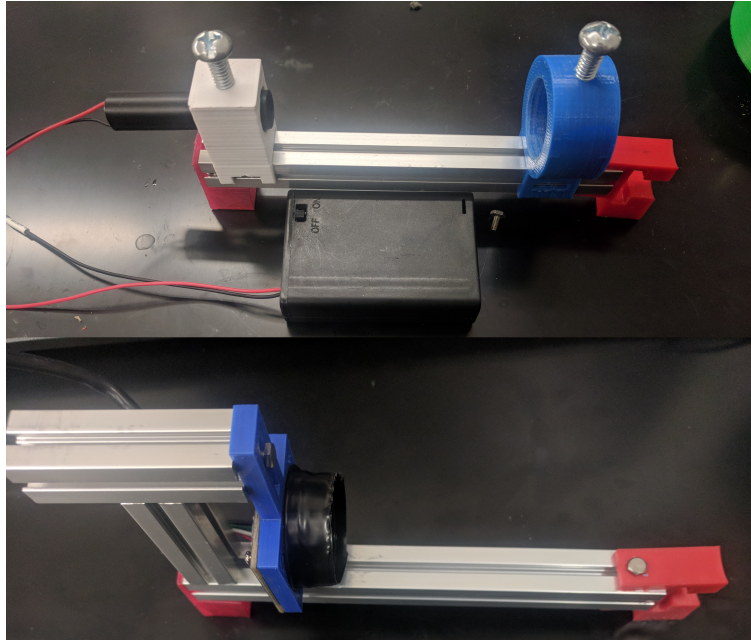


Figure 4: Top: the beam holding the laser and focusing lens. Bottom: the beam holding the camera and neutral density filter.

Each beam is a 15cm x 10mm x 10mm aluminum MakerBeam. Attached on the left side of each beam in Figure 4 is a foot used to keep the beams level with the central platform. On the right side of each beam is a 3D printed connector used to fasten the beams to the primary stage. The beams are capable of rotating around the axis that keeps these connectors in place, allowing a larger range of coupling angles for the laser-multilayer system.

The primary stage (see the green 3D printed fixture in Figure 5) acts as the center about which the incident beam can be coupled to the prism and then reflected. The design of this stage allows different types of multilayers to be used since the incident laser beam can be oriented at nearly any angle. The flowcell stage (see the blue 3D printed piece bolted into the primary stage in Figure 5) is a modular piece that is attached to the primary stage with four bolts. The prism, multilayer, and flowcell chamber are all strapped together on this stage via 3D printed braces and hex screws. The modular nature of this piece of the sensor is very valuable since multiple designs can be used to achieve the same goal and it only takes about an hour to print off each flowcell stage. When the braces are tightened there is no liquid loss at the interface during operation, however the chamber is made of PLA and liquid will leak through the plastic after a few hours.

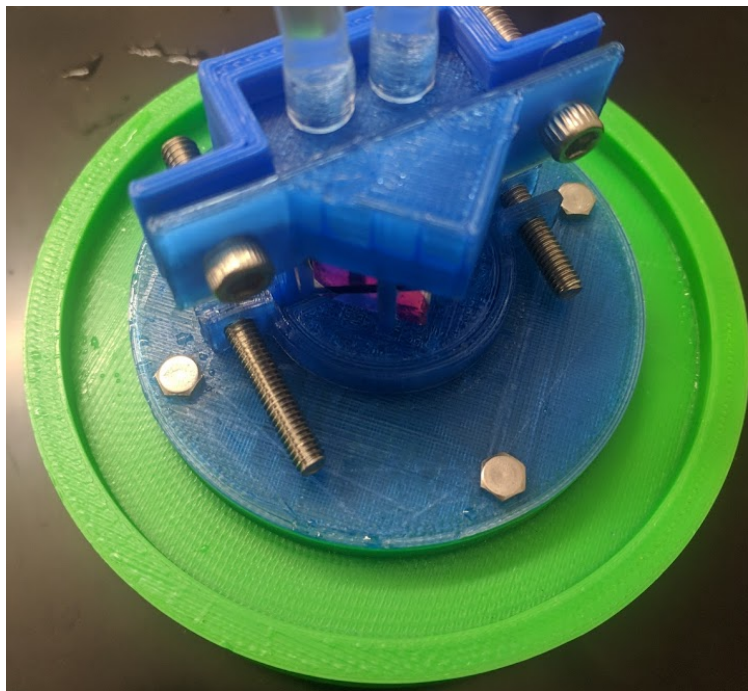


Figure 5: Primary stage and flowcell stage of our sensor. The green round 3D printed fixture underneath the flowcell is the primary stage which the two beams are attached to. The blue 3D printed piece mounted to the primary stage is the flowcell stage. The glass prism, multilayer, and flowcell chamber are attached atop the flowcell stage with the use of hex screws and 3D printed braces.

To flow liquids through the chamber the whole fixture must be water tight. To accomplish this we designed the flowcell so that a rubber gasket could be fit around the chamber.

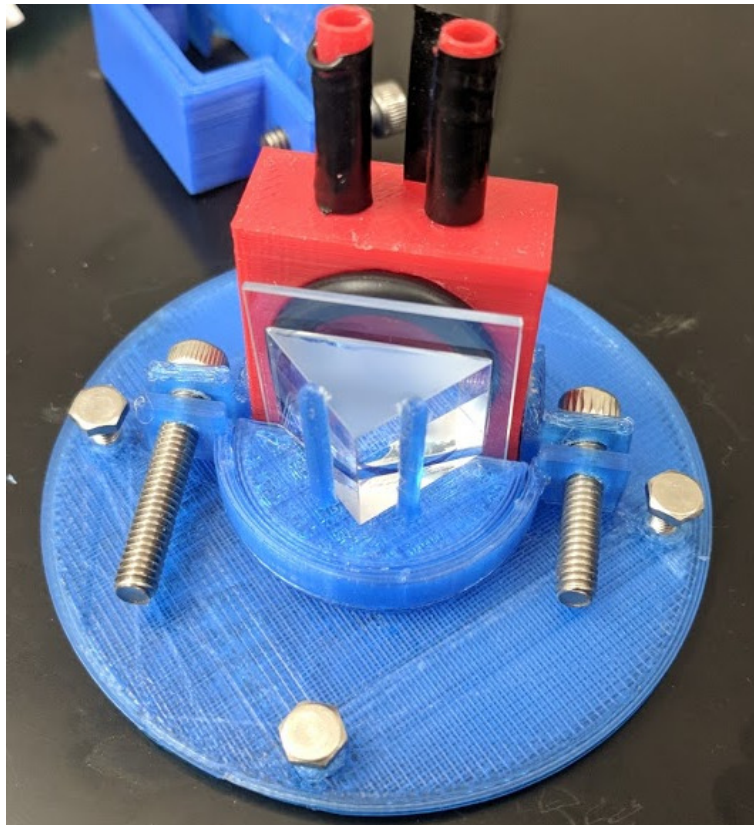
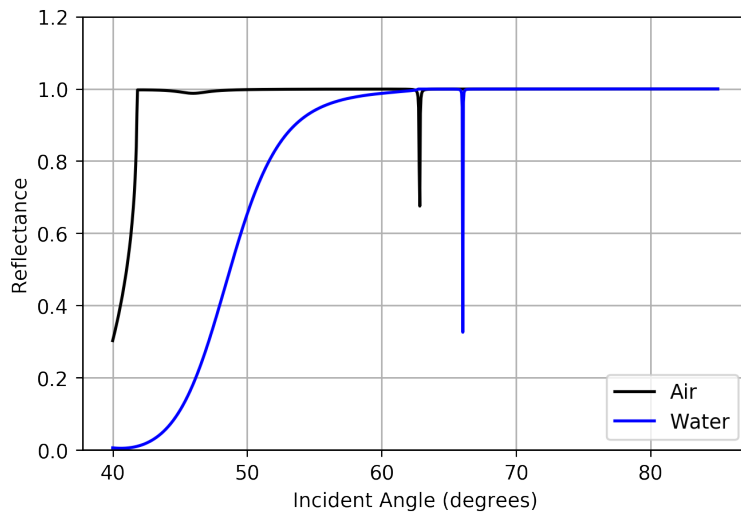


Figure 6: The flowcell stage, prism, multilayer and flowcell chamber. A rubber gasket is set in a groove around the chamber so that when the braces are tightened the interface between the multilar and flowcell is liquid tight.

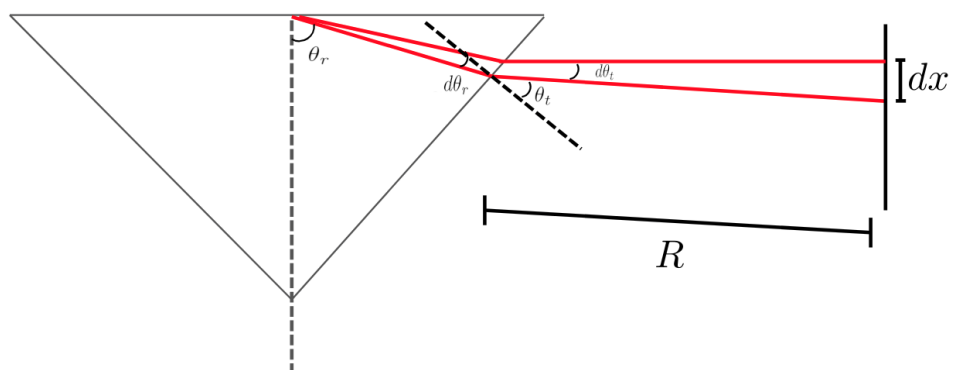
### III. Methods

To collect data from our biosensor we first prepare the flowcell chamber with the correct substrate or liquid that acts as our reference point for measuring changes in optical properties. After the chamber is prepared we then turn on the beam and rotate it until the special angle is reached.



As the index of refraction inside the flowcell chamber changes the dark band will translate left or right in our reflected image, depending on whether the index is increasing or decreasing. The shift in location of the band, in pixels, corresponds to an angular shift in the part of the reflected beam giving rise to the dark band. This is shown clearly in ?? as we see that a change from an index of 1.00 (air) to 1.33 (water) corresponds to an angular shift of about  $3^\circ$ .

Using the calculated data we can build a model to relate the index of refraction in the chamber to a shift in pixels on our CCD. To construct this relation we require Snell's law and some geometry. Using the classic formula for arclength and the diagram below we find:



$$dx = R d\theta_t$$

Using Snell's law we find

$$\theta_t = \arcsin(\sin(n_g \theta_r))$$

Which implies that

$$d\theta_t = d(\arcsin(n_g \sin \theta_r))$$

$$= \frac{n_g \cos \theta_r}{\sqrt{1 - n_g^2 \sin^2(\theta_r)}} d\theta_r$$

This leaves us with the relation between pixel shift and angular shift:

$$dx = \frac{R n_g \cos \theta_r}{\sqrt{1 - n_g^2 \sin^2(\theta_r)}} d\theta_r \quad (1)$$

Numerically we can determine the relationship between the reflected angle and the index inside the chamber. I wrote a python program to do just that for our multilayer, assuming the chamber is initially filled with water, and a graph of mode position ( $\theta_r$ ) vs index of refraction is plotted below.

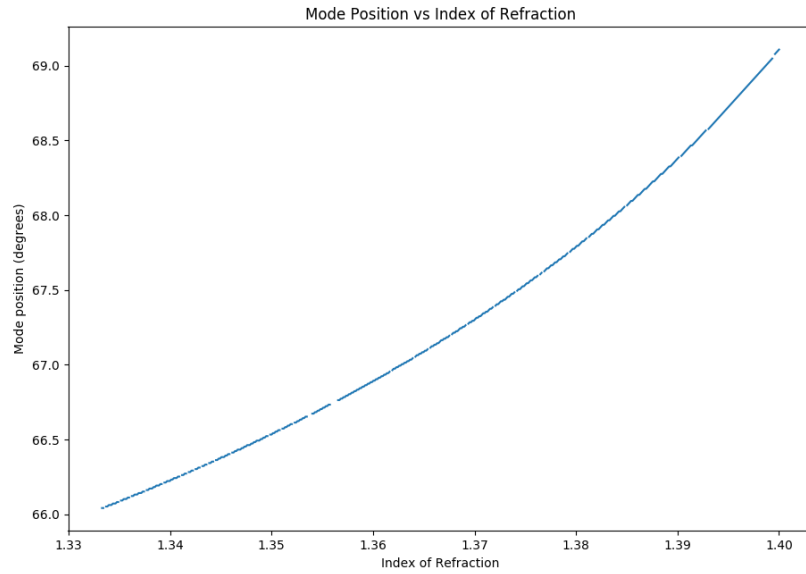


Figure 7: The theoretical relation between the angular position of the mode and the index of refraction inside the flowcell chamber.

## IV. RESULTS

The table in Figure 8 lists the mixtures of ethanol used to test for a change in index of refraction. The plot below shows the different indices of refraction corresponding to mixture A being injected over the interval [25, 55]. Similarly mixture B was injected over the interval [70, 90], and mixture C over [100, 150]. After the mixtures have time to settle in the chamber, they are flushed out with the same deionized water used to indicate the baseline mode position. Upon injecting a mixture with a higher index into the chamber we notice that the mode position shifts, as expected.

Using this data we can acquire a value of an index shift per pixel shift to quantify the sensitivity of the sensor. All of the mixtures used for testing have indices between 1.3380 and 1.3464, meaning that when the pixel shift of each mixture is plotted against the index of each we should expect a linear graph (see Figure 7) since small variations in reflected angle will yield a proportional shift in pixels. By extrapolating the data provided in the figure below we find that a shift in one pixel corresponds to a shift of about 0.0018 in index of refraction. This level of sensitivity exceeds the necessary sensitive to detect surface loading [?].

| Mixtures        | A      | B      | C      |
|-----------------|--------|--------|--------|
| Ethanol (ml)    | 10.0   | 20.0   | 30.0   |
| Water (ml)      | 100.0  | 100.0  | 100.0  |
| Index           | 1.3380 | 1.3418 | 1.3450 |
| Pixel Shift     | 80.0   | 135.0  | 245.0  |
| Change in Index | 0.0049 | 0.0052 | 0.0119 |

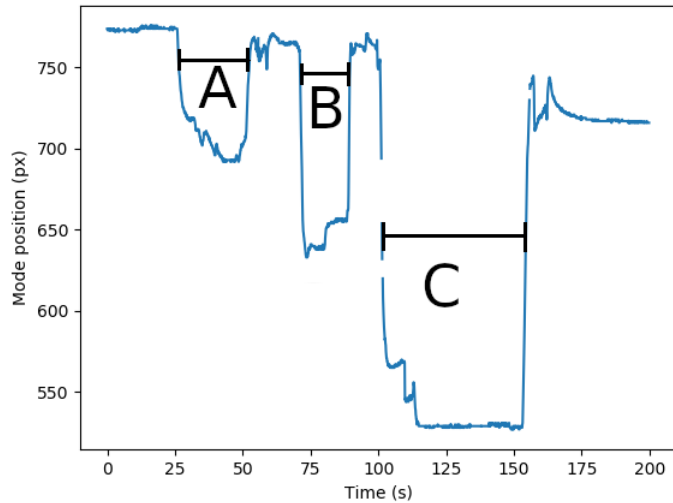


Figure 8: Index shift measurements for ethanol.

| Mixtures        | A      | B      | C      |
|-----------------|--------|--------|--------|
| Acetone (ml)    | 10.0   | 20.0   | 30.0   |
| Water (ml)      | 100.0  | 100.0  | 100.0  |
| Index           | 1.3384 | 1.3430 | 1.3464 |
| Pixel Shift     | 111.5  | 206.0  | 292.5  |
| Change in Index | 0.0052 | 0.0098 | 0.0132 |

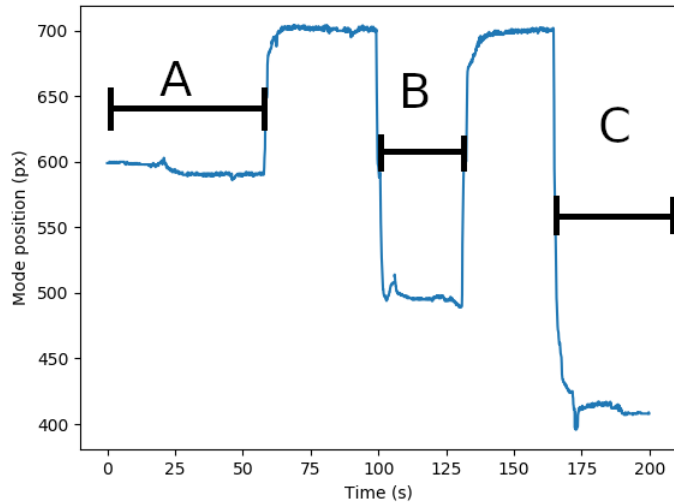


Figure 9: Index shift measurements for acetone.

| Mixtures           | A      | B      | C      |
|--------------------|--------|--------|--------|
| 70% Isop Alc. (ml) | 10.0   | 20.0   | 30.0   |
| Water (ml)         | 100.0  | 100.0  | 100.0  |
| Index              | 1.3398 | 1.3412 | 1.3447 |
| Pixel Shift        | 84.5   | 164.5  | 223.0  |
| Change in Index    | 0.0066 | 0.0080 | 0.0115 |

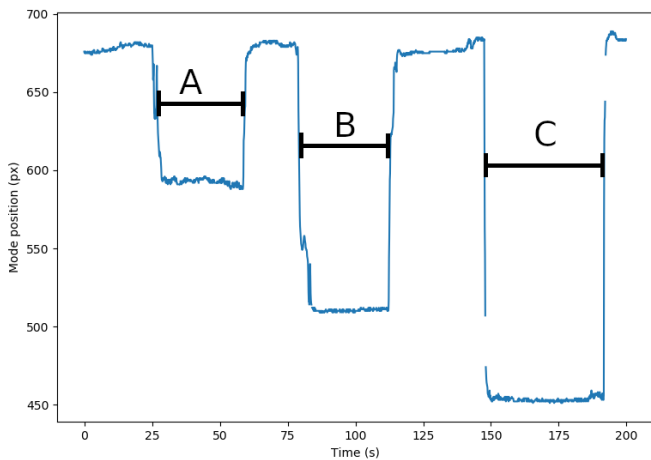


Figure 10: Index shift measurements for 70% isopropyl alcohol.

## V. CONCLUSION

In conclusion, this is a fine alternative to traditional flowcell sensors on the market. The only parts that need to be bought are the multilayers, a low power laser, a focusing lens, and a CCD. The rest of the parts can be 3D printed. The sensor does have a few issues, however. The flowcell itself is not quite water tight. This could be solved by either machining the flowcell or coating the chamber with a water tight sealant. Some multilayers may have coupling angles that are awkward to reach with the current design, however the modular nature of the flowcell stage can aid in reaching the coupling angle. In addition to modifying the flowcell stage, a hemispherical prism could be used in place of the right triangular prism used in our apparatus. The largest uncertainty of our device comes from the error in our ability to measure the pixel shift of the surface mode. At the moment a nine by nine gaussian blur is used to smooth out the image of the surface mode leaving us with an uncertainty in the mode position of about  $\pm 9$  pixel .

## VI. References

- [1] J. Homola, S. S. Yee, and G. Gauglitz, "Surface plasmon resonance sensors," *Sensors and Actuators B: Chemical*, vol. 54, no. 1-2, pp. 3–15, 1999.
- [2] W. M. Robertson, "Experimental measurement of the effect of termination on surface electromagnetic waves in one-dimensional photonic bandgap arrays," *Journal of Lightwave Technology*, vol. 17, no. 11, pp. 2013–2017, 1999.